PNAS
www.pnas.org

Supplementary Information for

Title: Power-law tail in lag time distribution underlies bacterial persistence.

Author: Emrah Şimşek and Minsu Kim

The corresponding author: Minsu Kim

Email: minsu.kim@emory.edu

This PDF file includes:

Supplementary Method

Supplementary Dataset

Supplementary Figures 1 to 4

Supplementary Note 1 and 2

Supplementary Table

Supplementary References

Supplementary Information Text

Supplementary Method

Colony forming unit (CFU) assay

For Fig. 1, CFU assays were performed to determine a time-dependent killing curve of a bacterial population exposed to ampicillin. Cells were cultured and starved as described in the Method section. On the third day of starvation (67.7 - 70.5 hours), cells were transferred to a fresh pre-warmed rich (LB) medium with 100 µg/ml ampicillin (time zero), and incubated at 37 °C. At different time points *t*, a fixed volume was spread on LB agar plates (100 × 15 mm Petri dish) containing no ampicillin after appropriate serial dilutions. The plates were then incubated at 37 °C overnight. Next morning, we counted visible colonies (which varied between 30 – 300) on the LB agar plates and determined the CFUs per milliliter. For each time point *t*, at least two biological replicates were performed, and their mean (data points) and standard deviation (error bars) were reported in Fig.1. Within each biological replicate, at least four technical replicates were performed, and their average was used.

Single-cell level observation of lag time using a microscope

Our microscope configuration was described in the Method section. For Fig. 2, on the third day of starvation (70.1 - 73.7 hours, as described in the Method section), a 5 µl aliquot of cells was spread onto a pre-warmed 35 mm glass-bottom Petri dish (InVitro Scientific). Then, a pre-warmed LB agarose pad with an approximate volume of 2.4 ml containing ampicillin (100 µg/ml final concentration) was gently placed on top of the cells such that the pad covered the entire bottom surface of the dish. The dish was then sealed with parafilm to limit water evaporation and immediately moved to a pre-warmed (37 °C) microscope for time-lapse imaging. An oil immersion 60× objective was used to acquire phase-contrast images of the cells.

The lag time of individual cells (Fig. 2) was measured using a time-lapse microscopy. Cells were imaged at different time points, their size was calculated using MicrobeJ, and the duration for which a cell maintained its size was used to determine its lag time. To visualize a power law, we logarithmically binned the data shown in Fig. 2a, producing Fig. 2b. Briefly, defining the bottom of the lowest bin and the ratio of the widths of successive bins as x_{min} and a, the k^{th} bin extends from $x_{k-1} = x_{min}\, a^{k-1}$ to $x_k = x_{min}\, a^k$. Importantly, Fig. 2b represents probability distribution, and thus the number of observations made within each bin was normalized by the bin width. For triangles, x_{min} = 70 min and a = 2. For rectangles, x_{min} = 140 min and a = 1.5.

Single-cell level determination of time delay in ampicillin-killing of growing cells

To determine the time delay (Supplementary Fig. 2), cell culture was first maintained in exponential growth phase for at least nine doublings until it reached OD_{600} = 0.2 - 0.3 in LB broth, and then a 4 µl aliquot was spread onto a pre-warmed 35 mm glass-bottom Petri dish (InVitro Scientific). Then, a pre-warmed LB agarose pad with an approximate volume of 2.4 ml containing ampicillin (100 µg/ml final concentration) was gently placed on top of the cells such that the pad covered the entire bottom surface of the dish. The dish was then sealed with parafilm to limit water evaporation and immediately moved to a pre-warmed microscope for time-lapse imaging at 37 °C. In this experiment, the LB agarose pad contained also propidium iodide (PI, Thermo-Fisher) at 4 µM of final concentration. An oil immersion 60× objective was used to acquire phase-contrast and red fluorescence images of the cells. Then, the distribution of time at which a cell got stained by PI or lost refractivity in its phase contrast image (i.e., lysed) (whichever comes first) was determined.

We additionally confirmed that PI is a good indicator for cell death by ampicillin; when we incubated cells with ampicillin and PI for 80 mins and spread them on an LB agar plate

containing no ampicillin, none of the PI stained (PI+) cells grew. A total number of ~25 PI+ ampicillin-affected cells were examined in five biological replicates.

Determination of values of τ_0, k, β, A_1 and A_2

Fig. 2a shows a semi-log plot of lag time probability distribution. Data below 105 min were fitted to a linear function, yielding $k = 0.063$ min^{-1} ($R^2 \sim 0.907$). Fig. 2b shows a log-log plot. This dataset was fitted to a linear function, yielding $\beta = -2.1$ ($R^2 \sim 0.977$). τ_0, A_1 and A_2 were determined using the following three equations. First, because the lag time probability distribution is continuous, $A_1 e^{-k\tau_0} = A_2 \tau_0^{\beta}$ in Eq .1. Second, its cumulative probability is equal to 1, i.e. $\int_0^{\tau_0} A_1 e^{-k\tau} d\tau + \int_{\tau_0}^{\infty} A_2 \tau^{\beta} d\tau = 1$. Here, $\int_0^{\tau_0} A_1 e^{-k\tau} d\tau$ is equal to the fraction of normal cells, which we empirically found to be 0.98 (from the data presented with triangles and squares in Fig. 2a); thus $\int_0^{\tau_0} A_1 e^{-k\tau} d\tau = 0.98$. Solving these three equations, we obtained $\tau_0 = 93$ min, $A_1 = 0.062$ min^{-1} and $A_2 = 2.4$ min$^{1.1}$.

Determination of these parameters by fitting the time-dependent killing curve

The following ranges for the model parameters were explored using a custom-built MATLAB code; k (1/min) = [0.010, 0.200] with 0.001 increments, β = [-3.00, -1.51] with 0.01 increments, Δ (min) = [60, 200] with increments of one, and τ_0 (min) = [10, 270] with increments of one. For each set of parameters (k, β, Δ, τ_0), $\int_0^{\tau_0} A_1 e^{-k\tau} d\tau + \int_{\tau_0}^{\infty} A_2 \tau^{\beta} d\tau = 1$ and $A_1 e^{-k\tau_0} = A_2 \tau_0^{\beta}$ were solved for A_1 and A_2. Using these values, we then computed the fraction of viable cells, $g(t)$, and compared them with experimental values (time-dependent killing data). The best-fit parameter values are shown in Supplementary Table.

Supplementary Dataset

Below we provide the values for all our data.

Data presented in Fig. 1: Data points are the arithmetic mean. The error bars represent the standard deviation of the values reported below for three biological replicate experiments.

Biological Replicate #1		**Biological Replicate #2**		**Biological Replicate #3**	
Time (min)	N_{CFU}	**Time (min)**	N_{CFU}	**Time (min)**	N_{CFU}
25	1.00×10^{0}	26	1.00×10^{0}	23	1.00×10^{0}
56	1.19×10^{0}	55	9.37×10^{-1}	53	1.07×10^{0}
84	1.13×10^{0}	85	6.62×10^{-1}	83	6.70×10^{-1}
113	3.08×10^{-1}	114	2.83×10^{-1}	112	2.32×10^{-1}
142	5.14×10^{-2}	143	3.77×10^{-2}	143	2.29×10^{-2}
212	2.09×10^{-2}	217	1.06×10^{-2}	213	7.88×10^{-3}
322	1.14×10^{-2}	330	5.03×10^{-3}	325	4.19×10^{-3}
447	8.37×10^{-3}	447	3.01×10^{-3}	N/A	N/A
539	6.66×10^{-3}	541	2.25×10^{-3}	N/A	N/A
650	5.04×10^{-3}	652	1.64×10^{-3}	657	1.23×10^{-3}
943	2.55×10^{-3}	947	7.47×10^{-4}	N/A	N/A

Data presented in Fig. 2a.

Here, the data obtained from three independent experiments were presented by three different symbols; circles, triangles and squares. For each independent experiment, we took time-lapse images of bacterial cells at various time points (T_1, T_2, …, T_i, T_{i+1}…) and counted the number of bacterial cells that resumed growth (N_i) between T_i and T_{i-1}. In Fig. 2, lag time, τ, represents the middle points of the bins, $(T_i + T_{i-1})/2$. Probability distribution $f(\tau)$ represents probability divided by the bin width $N_i /(\Sigma N_i)/(T_i - T_{i-1})$.

Circles		**Triangles**		**Squares**	
Imaging time point, T_i (min)	**Number of observations, N_i**	**Imaging time point, T_i (min)**	**Number of observations, N_i**	**Imaging time point, T_i (min)**	**Number of observations, N_i**
30	462	69	1372	120	10077
60	81	84	19	140	16
90	6	105	9	200	66
120	2	124	8	260	39
		144	1	320	19
		164	2	380	9
		189	2	440	4
		227	2	500	6
		346	2	560	5
		403	2	620	2
		522	1	680	6
		644	1	740	2
		827	1	800	1
		883	1	860	3
		947	1	920	1
		1188	1	980	3

				1040	2
				1160	2
				1220	1

Data presented in Fig. 2b.

Logarithmic binning rules, as described in the Supplementary Method section, were applied to the data presented above for the triangles and squares in Fig. 2a.

Triangles		**Squares**	
Logarithmically binned time point (min)	**Number of observations**	**Logarithmically binned time point (min)**	**Number of observations**
70	1372	140	10093
140	36	209	66
280	7	313	39
560	5	468	32
1120	4	700	18
2240	1	1047	10
		1565	5

Supplementary Figure 1. Early exponential decay of lag time distribution

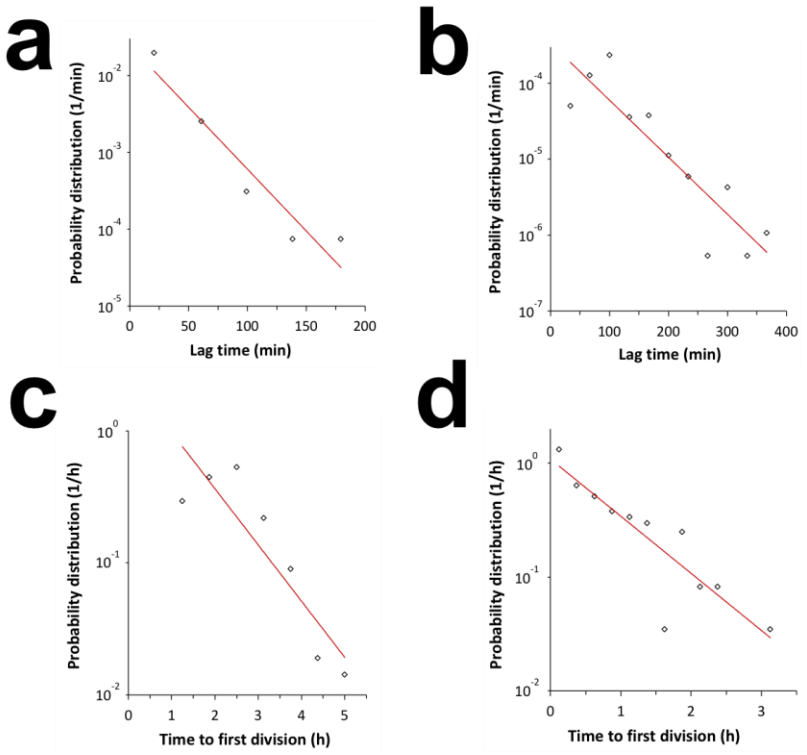

We observed an exponential decay in the early part of lag time probability distribution (Fig. 2). Previous population dynamic modeling studies often assumed that lag time distribution of bacterial cells exhibits an exponential decay [1,2]. Other experimental studies investigated two or three orders of magnitude decrease of lag time distribution (the range comparable to that of our early part of distribution where we observed an exponential decay). Here, we re-plotted the data of these experimental studies and fit them with an exponential function, which shows that an exponential decay is a good approximation. **a.** In our previous-published studies [3], *E. coli* cells were starved of carbon for eight hours, and then suspended in LB medium. Lag times of individual cells were determined by microscopy at 37 °C. The red straight line in a semi-log scale indicates an exponential decay with R^2 = ~ 0.917. Reprinted from ref. [3] (Sup. Fig. 13). **b.** In

the study by Levin-Reisman *et al*. [4] (Fig. 1d), *E. coli* cells were starved and suspended in a complex medium. Lag times of individual cells were determined by microscopy at 32 °C. The red straight line in a semi-log scale indicates an exponential decay with R^2 = ~ 0.802. Reprinted by permission from ref. [4], Springer Nature: Nature Methods, copyright (2010). **c.** In the study by Kutalik *et al*. [5] (Fig. 4), *Listeria innocua* cells were starved and suspended in complex medium. The time to the first division of individual cells was determined by microscopy at ambient temperature. The red straight line in a semi-log scale indicates an exponential decay with R^2 = ~ 0.802. Reprinted from ref. [5], Copyright (2005), with permission from Elsevier. **d.** In the study by Francois *et al*. [6] (Fig. 2), *Listeria monocytogenes* cells were starved and suspended in complex medium. The time to the first division of individual cells was determined by optical density measurements using microtiter plates at 30 °C. The red straight line in a semi-log scale indicates an exponential decay with R^2 = 0.775. Reprinted from ref. [6], Copyright (2005), with permission from Elsevier.

Supplementary Figure 2. Time delay of ampicillin killing

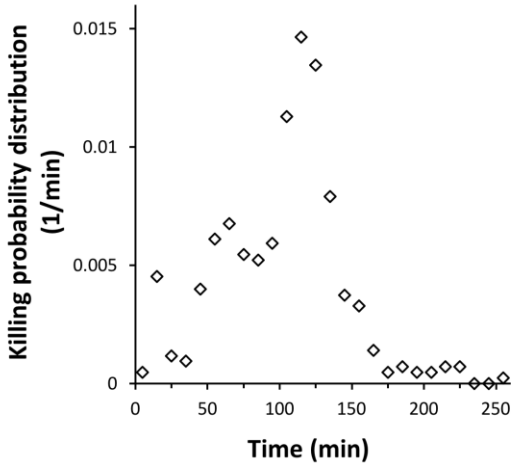

As described in the main text, we evaluated the time of ampicillin killing by exposing growing cells to ampicillin (100 µg/ml final concentration) and tracking propidium iodide (PI)-staining or the loss of cell refractivity (whichever comes first). Here, we plotted the distribution of ampicillin killing time, which showed that on average, it takes $\Delta = 102$ mins for ampicillin to kill growing cells. The distribution was obtained from two biological repeats. ~ 200 cells were examined within each biological repeat. Average killing time varied by less than 7 % across the two biological repeats when separately analyzed.

Supplementary Figure 3. Testing the effect of mutation on the time-dependent killing curve

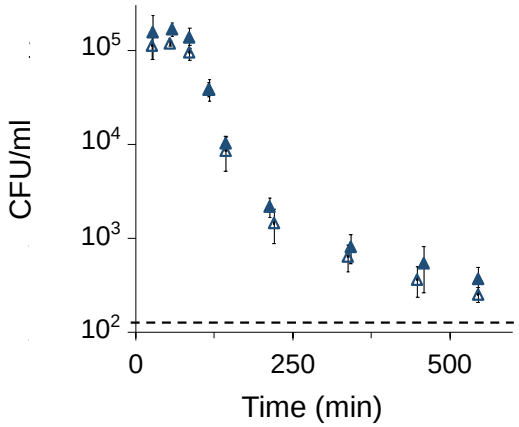

Cultures starved for long periods of time yield mutants, called the growth advantage in stationary phase (GASP). The appearance of GASP mutants is accompanied by an abrupt transition in the number of the colony-forming unit, N_{CFU}; N_{CFU} initially decreasing at a constant rate due to starvation reaches a plateau when GASP mutants appear. The timing of appearance of GASP mutants depends on the types of media used; for example, in Luria-Bertani (LB) media, they appear within several days of starvation [7], whereas they appear after ~ 30 days of starvation in minimal media [8]. In our experiments, we used minimal media, and cells were starved for ~ 3 days. Therefore, GASP mutants are unlikely to appear. Indeed, we did not observe such an abrupt transition in N_{CFU} (i.e., from a rapid decrease to a plateau) during our experiment (the N_{CFU} data are available in our previously-published article [3]), which suggests that GASP mutants have not appeared during our experiments.

In order to further ensure that our findings are not affected by mutation, we repeated the time-dependent killing curve measurement by using cells collected at the end of the experiments. First, as described in the main text, we measured a time-kill curve of a population exposed to

ampicillin (solid triangles). We then collected cells at the end of the experiments and then repeated the entire experiments with the collected cells (open triangles). Their time-kill curves were very similar, which suggests that our observation was not affected by mutation. We note that the same approach was previously taken by others in order to provide evidence that persisters are not mutants [9,10].

Supplementary Figure 4. Testing the effect of initial cell density on our observations

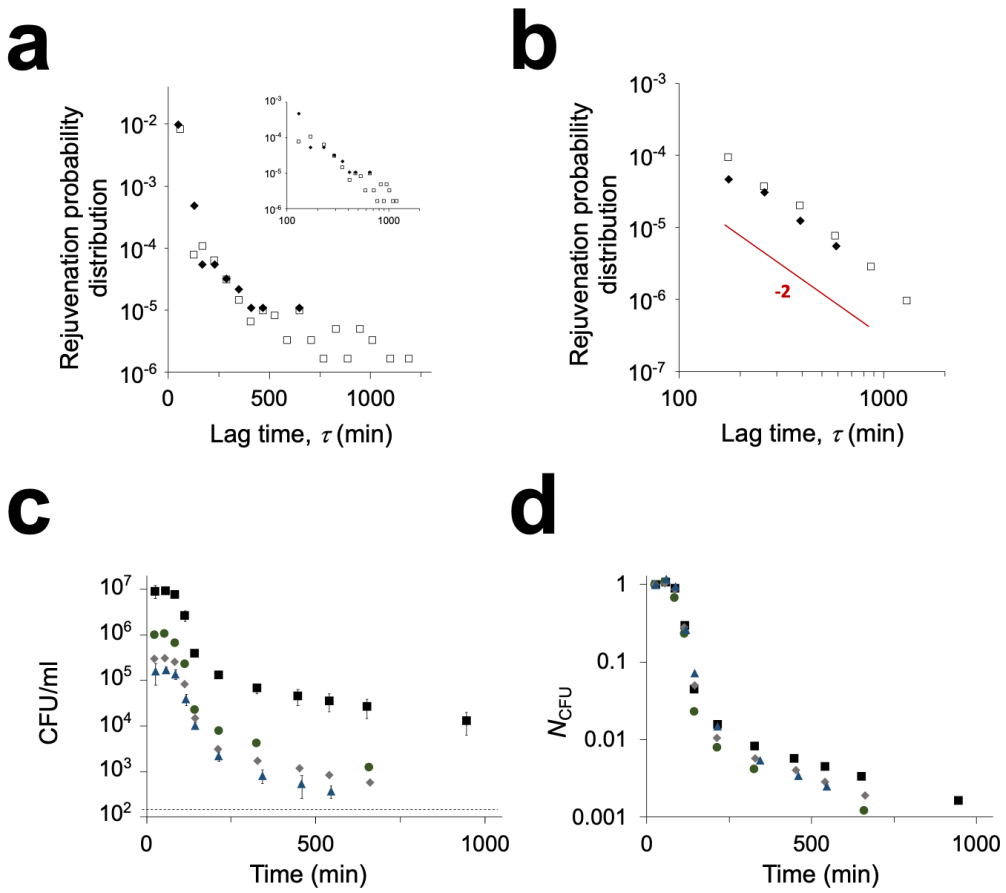

Persisters are typically present at very low frequency. Therefore, to reliably characterize persisters, we used a high initial cell density and monitored the lag time of ~12,800 cells in our original experiment, finding that the lag time distribution exhibits a power-law decay. Here, we performed more experiments to test whether our observation is affected by the initial cell density. In the new experiments, we lowered the initial density by 10-fold and monitored the lag time of ~1,600 cells. As was observed in the original experiments with a high cell density, the majority of cells rejuvenated during the early exponential decay phase, i.e., before τ_0 (= 93 min). Only 33 cells rejuvenated after τ_0. Interestingly, despite the issue of low sample size, their lag time distribution (black diamonds in Supplementary Fig. 4a) was comparable to the original

distribution with the high cell density (open square in Supplementary Fig. 4a, adopted from Fig. 2) and exhibited a power-law decay with the exponent of -2 (Supplementary Fig. 4b). Thus, lowering the cell density by 10-fold had no obvious effects on the power-law decay of the lag time distribution.

Additionally, we measured a time-dependent killing curve of a population exposed to ampicillin. In three different measurements, we lowered the initial density up to 100-fold and measured the viability of cells in the cultures (Supplementary Fig. 4c). In these experiments, low sample size remains a problem. For example, we could not measure points beyond 1,000 mins because the number of viable cells fell below the detection limit of plating. However, when we normalized the curves obtained with respect to their initial cell density, the normalized curves agreed with our original curve with the high initial cell density, exhibiting similar biphasic decays (Supplementary Fig. 4d).

In conclusion, while our new experiments with low cell densities suffer from low statistics (which was expected given a very low frequency of persisters), the new data suggest that lowering cell density has no obvious effects on our findings.

Supplementary Note 1: consideration of a finite population.

In the mathematical analysis of the power-law in the main text, the integral over *k* had an infinite upper hand limit (Eq. 8), which implies an infinite population (which is not realistic). The finiteness of a population would cut off the range of the integral of *k*. Importantly, because time *t* is the reciprocal of *k*, this cut-off will set the temporal range for which the power-law holds. Below, we elaborated this point by using a detailed mathematical analysis.

Initially, our original equation (Eq. 8) had an integral with infinite upper hand limit. If the integral has a finite upper limit (due to a finite population size), Eq. 8 would become

$$\overline{N}(\tau) \propto \int_0^{k_{\max}} k \cdot \exp(-\tau \cdot k) \cdot dk \quad . \qquad \text{(Eq. S1)}$$

The term on the right can be described by

$$\int_0^{k_{\max}} k \cdot \exp(-\tau \cdot k) \cdot dk = -\frac{d}{d\tau} \cdot \int_0^{k_{\max}} \exp(-\tau \cdot k) \cdot dk \,, \qquad \text{(Eq. S2)}$$

and

$$\int_0^{k_{\max}} \exp(-\tau \cdot k) \cdot dk = \frac{1}{\tau} \cdot \left[1 - \exp(-\tau \cdot k_{\max})\right]. \qquad \text{(Eq. S3)}$$

If $\tau \cdot k_{\max} >> 1$ or $\tau >> 1/k_{\max}$, $\exp(-\tau \cdot k_{\max})$ in the right term of Eq. S3 is approximated to be zero. Thus, Eq. S1 becomes $\overline{N}(\tau) \propto \frac{1}{\tau^2}$.

Therefore, the aforementioned temporal range ($\tau >> 1/k_{\max}$) sets the lower temporal bound for which the power-law is valid. In our experiments, we observed that the power law begins at τ ~100 mins, which suggests that $k_{\max} >> 1/$ (100 mins).

We can extend this analysis for the upper temporal bound of the power-law by including the lower hand limit of the integral in Eq. S1. With the lower hand limit, we have

$$\overline{N}(\tau) \propto \int_{k_{\min}}^{k_{\max}} k \cdot \exp(-\tau \cdot k) \cdot dk \ . \qquad \text{(Eq. S4)}$$

The right term of Eq. S4 is

$$\int_{k_{\min}}^{k_{\max}} k \cdot \exp(-\tau \cdot k) \cdot dk = -\frac{d}{d\tau} \cdot \int_{k_{\min}}^{k_{\max}} \exp(-\tau \cdot k) \cdot dk \ , \qquad \text{(Eq. S5)}$$

and

$$\int_{k_{\min}}^{k_{\max}} \exp(-\tau \cdot k) \cdot dk = -\frac{1}{\tau} \cdot \left[\exp(-\tau \cdot k)\right]_{k_{\min}}^{k_{\max}} = \frac{1}{\tau} \cdot \left[\exp(-\tau \cdot k_{\min}) - \exp(-\tau \cdot k_{\max})\right]. \qquad \text{(Eq. S6)}$$

If $\tau \cdot k_{\min} << 1$ but $\tau \cdot k_{\max} >> 1$, i.e., $1/k_{\max} << \tau << 1/k_{\min}$, Eq. S6 becomes

$\int_{k_{\min}}^{k_{\max}} \exp(-\tau \cdot k) \cdot dk \approx \frac{1}{\tau}$, and thus, $\overline{N}(\tau) \propto \frac{1}{\tau^2}$. In our experiments, the power-law was observed up to nearly 2,000 mins, meaning $k_{\min} << 1/$ (2,000 mins)

In conclusion, the finiteness of a population will set the temporal range for which the power-law holds.

Supplementary Note 2: consideration of a non-uniform distribution of *k*.

In the main text, we assumed a uniform distribution of k to provide an intuitive explanation of the observed power-law decay with the exponent of –2. Here, we want to test whether this assumption is necessary to explain this power-law decay. We will consider a non-uniform distribution of k by including a weighting factor $h(k)$. With this weighting factor, Eq. 8 in the main text becomes

$$\overline{N}(\tau) \propto \int_0^\infty h(k) \cdot k \cdot \exp(-\tau \cdot k) \cdot dk \ . \qquad \text{(Eq. S7)}$$

When k is uniformly distributed, $h(k)$ is constant. To address the question whether this assumption is necessary, it would be convenient to consider $h(k)$ that 1) changes from a uniform to non-uniform distribution as a parameter in the function is tuned and 2) is simple enough so that the analytical solution (Eq. S7) can be derived. One such function is $h(k) = a \cdot \exp(-a \cdot k)$. In the limit of $a \to 0$, $h(k)$ converges to a uniform distribution. As a gets larger, the function becomes more steeply varing.

With $h(k) = a \cdot \exp(-a \cdot k)$, the solution of Eq. S7 is

$$\overline{N}(\tau) \propto \frac{1}{(a+\tau)^2} \ , \qquad \text{(Eq. S8)}$$

which will converge to $\overline{N}(\tau) \propto \frac{1}{\tau^2}$ when $\tau >> a$. It means that if a is small, we will observe a power-law decay with the exponent of −2 over a wide temporal range. As a gets larger, the beginning part of the curve will deviate from, but the tail of the curve will exhibit a power-law decay with the exponent of −2.

To ensure that this conclusion is not specific to an exponential distribution of k, we also considered a linear function, $h(k) = \frac{2a}{b^2} \cdot (b - a \cdot k)$. In the limit of $a \to 0$, $h(k)$ converges to a uniform distribution. With this function, the solution of Eq. S7 is

$$\overline{N}(\tau) \propto \frac{-2a + b\tau}{\tau^3} + \frac{(2a + 2\tau)}{\tau^3} \exp(-\frac{b}{a} \cdot \tau) \ . \qquad \text{(Eq. S9)}$$

(The integral in Eq. S7 was performed from 0 to $\frac{b}{a}$ in this case because, above this upper limit, $h(k)$ becomes negative). The solution Eq. S9 converges to $\overline{N}(\tau) \propto \frac{1}{\tau^2}$, if $\tau >> \frac{a}{b}$. Therefore, the message is the same as above. If $\frac{a}{b}$ is small (compared to τ), we will observe a power-law decay with the exponent of –2 over a wide temporal range. As $\frac{a}{b}$ gets larger, the beginning part of the curve will deviate from, but the tail of the curve will exhibit a power-law decay with the exponent of –2. Therefore, the power-law decay with the exponent of –2 can emerge in long time regime even when the distribution of *k* is not uniform.

Indeed, in our experiments, we observed the power-law in the temporal region greater than 100 mins (Fig. 2). In fact, while power-law distribution is a widespread feature in many stochastic processes, observed in physics, ecology, earth sciences and social sciences, these empirical distributions typically exhibit a power-law decay only in the tail [11]. Our analysis above could provide one mechanism of why this is the case.

But, that is not to say that all non-uniform functions of $h(k)$ generate the power-law of –2 in the tail. For example, if $h(k) \propto \frac{1}{k}$, i.e., the density of cells diverges to infinity as $k \to 0$, $\overline{N}(\tau) \propto \frac{1}{\tau}$. If $h(k) \propto k \cdot \exp(-k/b)$, a gamma distribution where the density of cells converges to zero as $k \to 0$, the solution of Eq. S7 is $\overline{N}(\tau) \propto \frac{1}{(1/b+\tau)^3}$. In these cases, even in the long time regime, the power-law decay with the exponent of –2 will not emerge.

We believe that it is beyond the scope of this work to identify the exact mathmatical condition for which the power-law decay with the exponent of –2 emerges. However, our analysis reveals that a uniform distribution of k is not absolutely needed to observe a power-law decay with the exponent of –2.

Supplementary Table. The parameters of our model describing the time-dependent killing curve

Parameter	Empirical	Best fit
k	0.063 min^{-1}	0.105 min^{-1}
β	-2.1	-2
Δ	102 min	100 min
τ_0	93 min	47 min
A_1	0.062 min^{-1}	0.10211 min^{-1}
A_2	2.4 $min^{1.1}$	1.6219 min

Our mathematical model for the time-dependent killing curve is given by Eq. (1-3) in the main text. The parameters of this model were first estimated by analyzing the empirical data (the left column; see the main text for details). We then determined the goodness of the fit with these parameters by using a logarithmic least squares formula $S = \sum_{i=1}^{n=11} \left(\log_{10} g_{\text{data}}(t_i) - \log_{10} g_{\text{model}}(t_i) \right)^2$, where n represents the data points in Fig. 1 or 3 ($S = 3.26 \times 10^{-1}$). We then varied the parameter values and found the values minimizing S (the right column, $S = 3.03 \times 10^{-2}$).

Supplementary References

1 Baranyi, J. Stochastic modelling of bacterial lag phase. *Int J Food Microbiol* **73**, 203-206, doi:10.1016/S0168-1605(01)00650-X (2002).

2 Baranyi, J. & Pin, C. Estimating bacterial growth parameters by means of detection times. *Appl Environ Microbiol* **65**, 732-736 (1999).

3 Şimşek, E. & Kim, M. The emergence of metabolic heterogeneity and diverse growth responses in isogenic bacterial cells. *ISME J* **12**, 1199-1209, doi:10.1038/s41396-017-0036-2 (2018).

4 Levin-Reisman, I. *et al.* Automated imaging with ScanLag reveals previously undetectable bacterial growth phenotypes. *Nat Methods* **7**, 737-739, doi:10.1038/nmeth.1485 (2010).

5 Kutalik, Z., Razaz, M., Elfwing, A., Ballagi, A. & Baranyi, J. Stochastic modelling of individual cell growth using flow chamber microscopy images. *Int J Food Microbiol* **105**, 177-190, doi:10.1016/j.ijfoodmicro.2005.04.026 (2005).

6 Francois, K. *et al.* Modelling the individual cell lag phase: effect of temperature and pH on the individual cell lag distribution of Listeria monocytogenes. *Int J Food Microbiol* **100**, 41-53, doi:10.1016/j.ijfoodmicro.2004.10.032 (2005).

7 Finkel, S. E. Long-term survival during stationary phase: evolution and the GASP phenotype. *Nat Rev Microbiol* **4**, 113-120, doi:10.1038/nrmicro1340 (2006).

8 Vasi, F. K. & Lenski, R. E. Ecological strategies and fitness tradeoffs inEscherichia coli mutants adapted to prolonged starvation. *Journal of Genetics* **78**, 43-49, doi:10.1007/bf02994702 (1999).

9 Bigger, J. Treatment of Staphlococcal infections with penicillin by intermittent sterilisation. *Lancet* **244**, 497-500, doi:10.1016/S0140-6736(00)74210-3 (1944).

10 Keren, I., Kaldalu, N., Spoering, A., Wang, Y. & Lewis, K. Persister cells and tolerance to antimicrobials. *FEMS Microbiol Lett* **230**, 13-18, doi:10.1016/S0378-1097(03)00856-5 (2004).

11 Newman, M. E. J. Power laws, Pareto distributions and Zipf's law. *Contemp Phys* **46**, 323-351, doi:10.1080/00107510500052444 (2005).